J. Magn. Soc. Jpn., **40**, 8-12 (2016) <Paper>

The hysteresis properties analysis of Fe-4 wt% Si prepared by high purity metallurgy

Z. Lei, T. Horiuchi, I. Sasaki, C. Kaido*, M. Takezawa**, S. Hata***, Y. Horibe**, T. Ogawa****, H. Era**
Kyushu Institute of Technology, *2-4 Hibikino, Wakamatsu-ku, Kitakyushu-shi, Fukuoka, 808-0196, Japan*
*National Institute of Technology, Kitakyushu College, *5-20-1 Shii, Kokuraminami-ku, Kitakyushu-shi, Fukuoka, 802-0985, Japan*
**Kyushu Institute of Technology, *1-1 Sensui-cho, Tobata-ku, Kitakyushu-shi, Fukuoka, 804-0015, Japan*
***Kyushu University, *6-1 Kasugakoen, Kasuga, Fukuoka, 816-8580, Japan*
****Mechanics & Electronics Research Institute, Fukuoka Industrial Technology Center, *3-6-1, Norimatsu, Yahatanishi-ku, Kitakyushu-shi, 807-0831, Japan*

An investigation on the improvement in hysteresis properties of high purity Fe-4 wt% Si prepared by cold crucible levitation melting was presented compared with a Fe-0.1 wt% C- 4 wt% Si alloy formed by the identical process. The results showed that thin elongated carbon compounds were precipitated in both grains and grain boundaries of Fe-0.1 wt% C- 4 wt% Si sample observed by means of Kerr effect microscopy and STEM, leading to an apparent degradation in coercivity, permeability and hysteresis loss. With regard to hysteresis loss in Fe-4 wt% Si, it increases linearly with the increase of maximum magnetic flux density below 1.4 T, whereas for Fe-0.1 wt% C- 4 wt% Si, it behaves nonlinearly even at low maximum magnetic flux density and rises sharply with the increase of maximum magnetic flux density. Additionally, the precipitated carbon compounds in the grain boundaries change the morphology of the grain boundaries.

Key words: Fe-4 wt% Si, high purity, hysteresis loss, magnetic domain

1. Introduction

The iron loss P_{loss} of electrical steel can be divided into three components: hysteresis loss P_h, classical eddy current loss P_e, and anomalous loss P_a according to the equation:

$$P_{loss} = P_h + P_e + P_a \quad (1)$$

Among the three components, hysteresis loss is the fundamental loss in electrical steel, especially at high magnetic flux density in the typical frequency range of transformers. Hysteresis loss is typically associated with obstacles to domain wall motion such as grain boundaries, precipitates [1] and crystallographic orientations [2]. The improvement possibility in hysteresis loss of silicon iron alloy by reducing impurities has been recognized clearly [3, 4]. Kaido et al. [1] gave a theoretical calculation about the effect of the precipitates on the hysteresis loss by reducing impurities further than commercial non-oriented steel 35H210, and their results turned out that the influence can be decreased substantially to 1/4. On the other hand, the eddy-current loss is closely related to the domain size and mobility of domain wall [5], which also can be significantly influenced by the existence of precipitates, and its mechanism has been reported by several authors [6-8].

Most of the precipitates are originated from exterior impurities during a series of metallurgy processes and reduction of impurities is running up against potency in the conventional metallurgy processes. Therefore, in this current study, a method called cold crucible levitation melting (CCLM) was embraced to minimize the impurities in the ingots. The most important feature of CCLM is that the molten alloy can be levitated from the cold crucible by magnetic force, so as to reduce the impurities apparently by isolating the contamination from the crucible during melting [9]. Meanwhile, highly pure raw iron and silicon with a purity of 99.99 wt% and 99.999 wt% respectively were utilized to prepare the alloys.

In this paper, to clarify the potential of improvement in hysteresis properties by high purity, Fe-4 wt% Si alloy was firstly prepared by CCLM. Another Fe-4 wt% Si alloy with 0.1 wt% carbon added was also prepared as a comparison to reveal the effect of carbon on the magnetic properties and its interaction with domain structures. The permeability, coercivity and hysteresis loss of both alloys were studied. Additionally, the morphology of microstructure and the demagnetized domain structure were investigated by means of Kerr effect microscopy. The factors which influenced the hysteresis properties were discussed in detail by taking the domain structure and microstructure into consideration.

2. Materials and methods

Two kinds of Fe-4 wt% Si samples without and with addition of 0.1 wt% carbon were used for this study, identified as 4N and 3N. Two samples were both prepared from raw iron and silicon with a purity of 99.99 wt% and 99.999 wt% respectively in CCLM under high vacuum, except 3N with addition of 0.1 wt% carbon (99.999 wt%), which can be summarized as 4N (Fe-4 wt% Si) and 3N (Fe-0.1 wt% C-4 wt% Si). The detail of the identical CCLM furnace and its effect of impurities elimination, the homogeneity of element distribution can be found in the papers [10, 11]. Both the

samples were maintained at melted condition and stirred for about 20 min at approximately 1600 °C, then followed by furnace cooling to room temperature (without subsequent annealing).

Hysteresis loops were measured at maximum magnetization from approximately 0.5 T to 1.5 T, and 5000 A/m applied field on both 5-mm-thick ring samples of 35 mm inner and 45 mm external diameter. These tests were performed under direct current (DC) using a magnetization measurement instrument, and various hysteresis properties were calculated based on the hysteresis loops.

The samples for domain observation were cut from the ring samples. The thickness of both samples was 2.5 mm and they were both finely grounded with an adequate finish polish with 0.02 μm colloidal silica, so as to reduce the agitation of surface stress. The demagnetized domain structures were observed using Kerr effect microscopy. The determination of crystallographic direction and microstructure were performed by Electron Back-Scattered Diffraction (EBSD) equipped in a SU-70 Scanning Electron Microscopy and analyzed by Orientation Image Microscopy (OIM) software. The morphology of precipitates in 3N sample were observed by Scanning Transmission Electron Microscopy (STEM) equipped in the FEI TECNAI-F20 TEM, and its samples were prepared by ion milling after a mechanical polish to about 30 μm.

3. Results and Discussion

3.1. Hysteresis loop

The hysteresis loops in Fig. 1 show that 4N sample has better hysteresis properties with lower coercivity of 18 A/m compared with 76 A/m, and remanence of 0.32 T compared with 0.48 T of 3N. All of the compared data are summarized in Table 1. Additionally, 4N can be magnetized up to its

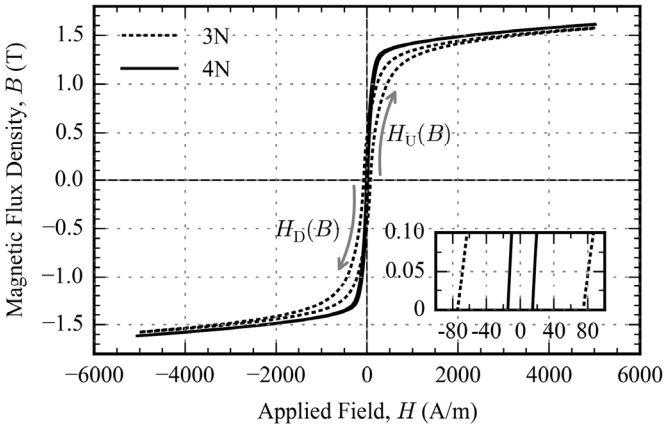

Fig. 1 DC hysteresis loops measured in 3N and 4N ring samples at maximum applied field H_m of 5000 A/m, associated with an inset for clarity of the coercivity and low magnetization part of hysteresis loops. Two arrows indicate the ascending branch $H_U(B)$ and descending branch $H_D(B)$ of hysteresis loops, respectively.

Table 1 Comparison of maximum magnetic flux density, coercivity, remanence and permeability of two samples at H_m = 5000 A/m

Hysteresis properties	4N	3N
Maximum magnetic flux density (T)	1.60	1.58
Remanence (T)	0.32	0.48
Coercivity (A/m)	18	76
Maximum permeability (H/m)	0.010	0.004
Relative maximum permeability	8000	3200

maximum permeability with value of 0.010 H/m at lower applied field of 30 A/m with comparison to 0.004 H/m of 3N at 120 A/m, which can be concluded that 4N sample can be easily magnetized to higher magnetization at lower applied field compared to 3N.

The hysteresis losses P_h in Fig. 2 are calculated from a series of hysteresis loops measured at maximum magnetic flux density B_m from approximately 0.5 T to 1.45 T, and its relationship with each corresponding B_m are shown in Fig. 2. It can be found that P_h of 4N is significantly lower than that of 3N in the whole range of B_m, especially at higher Bm. Additionally, the increase of P_h in 4N has a linear connection with B_m within the range of 0.5 and 1.45 T applied in the experiment, whereas P_h of 3N increases gradually at the low applied field and fast along with the increase of B_m.

During magnetization, it is generally agreed that 180° domain wall displacement takes place at low applied field which are mainly controlled by the second phases and grain size [12], and 90° domain wall displacement needs a fairly large magnetic field which are mainly controlled by the crystallographic texture [12]. The increment of hysteresis loss of high purity 4N sample only linearly relates with B_m, which is totally independent with the sample parameters such as grain size, texture, regardless of whether on the condition of 180° or 90° domain wall displacement stage. However, the

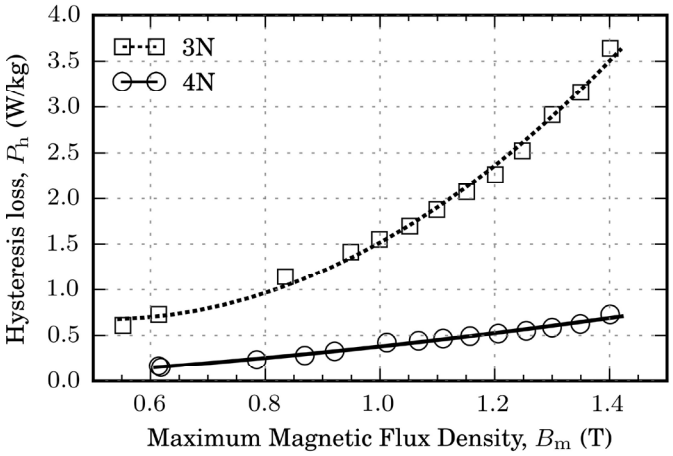

Fig. 2 Comparison of relationship of maximum flux density B_m (less than 1.45 T) and hysteresis loss P_h in 3N and 4N samples.

increment of hysteresis loss in 3N samples reveals its significant sensitivity on the structural parameters. During the 180° domain wall displacement stage at B_m lower than 0.6 T, the increment of hysteresis loss is linear without relying much on the structural variation, but at the 90° domain wall displacement stage, the energy loss dissipated by the motion of domain wall increases aggressively.

As known, hysteresis loss for ferromagnetic material is equivalent to the area of hysteresis loop, that is, $P_h = \oint HdB$. The integration can also be treated as the summation of slices of width of hysteresis loop mathematically. Each individual width $H_{CB}(B)$ of hysteresis loop can be defined as the difference of the ascending branch $H_U(B)$ and the descending branch $H_D(B)$ (see Fig. 1) at a specific magnetization B according to Eq. 3 [1]:

$$H_{CB}(B) = H_U(B) - H_D(B) \quad (3)$$

The variation of calculated $H_{CB}(B)$ as a function of B in the hysteresis loops of the two samples are shown in Fig. 3. It can be seen that $H_{CB}(B)$ maintains constantly till magnetization up to 1.2 T, then slightly increases and start to decrease afterwards in 4N sample, which is in accordance with the results of Fig. 2. As a comparison, $H_{CB}(B)$ of 3N approximately maintains as a small constant below magnetization of 0.6 T, then starts to grow gradually and finally increases abruptly to a very large value and start to decrease afterwards. This difference of hysteresis loop width during magnetization between those two samples will be discussed in the following sections by combining with the morphology of precipitates, crystallographic texture, grain and domain structure.

3.2. Effect of microstructure and phase

The phase, grain morphology and orientations of part of the two rings samples are observed by EBSD and some of the results are shown in Fig. 4. By summarizing all the results, the structure of near equiaxed grains exist in both of the samples and their average sizes are similar, which are approximately 5 mm, and the orientations of grains are random without any preferred orientations found (Fig. 4 (a) and (c)). Therefore, the influence of grain size below 0.6 T (180° domain wall displacement stage), and the influence of crystallographic orientations on the difference of hysteresis loop width above 0.6 T (90° domain wall displacement stage) in Fig. 3 can be ignored. So the big differences on hysteresis properties between the two samples are roughly considered as a consequence of the existence of precipitates introduced in by carbon concentration. The morphology of the grains in 4N (Fig. 4 (b)) is irregular polyhedron by the equilibrium growth of adjacent grains, whereas near-polyhedron in 3N (Fig. 4 (d)) with the addition influence of the carbon precipitates. On the other hand, only A2 base phases exist in

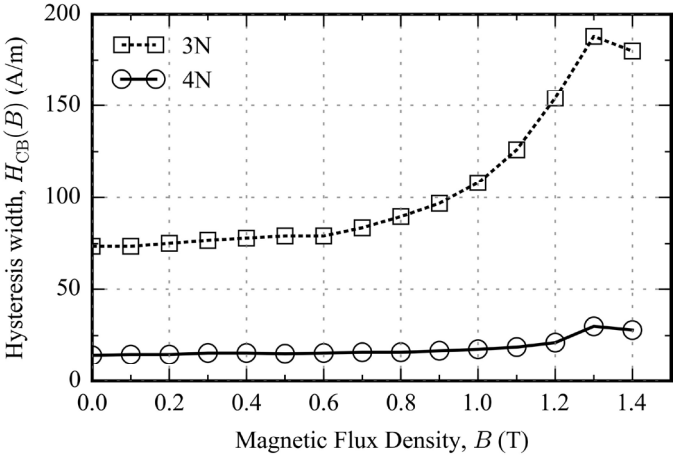

Fig. 3 Relationship of width $H_{CB}(B)$ of hysteresis loop at series of magnetic flux density B in 3N and 4N samples.

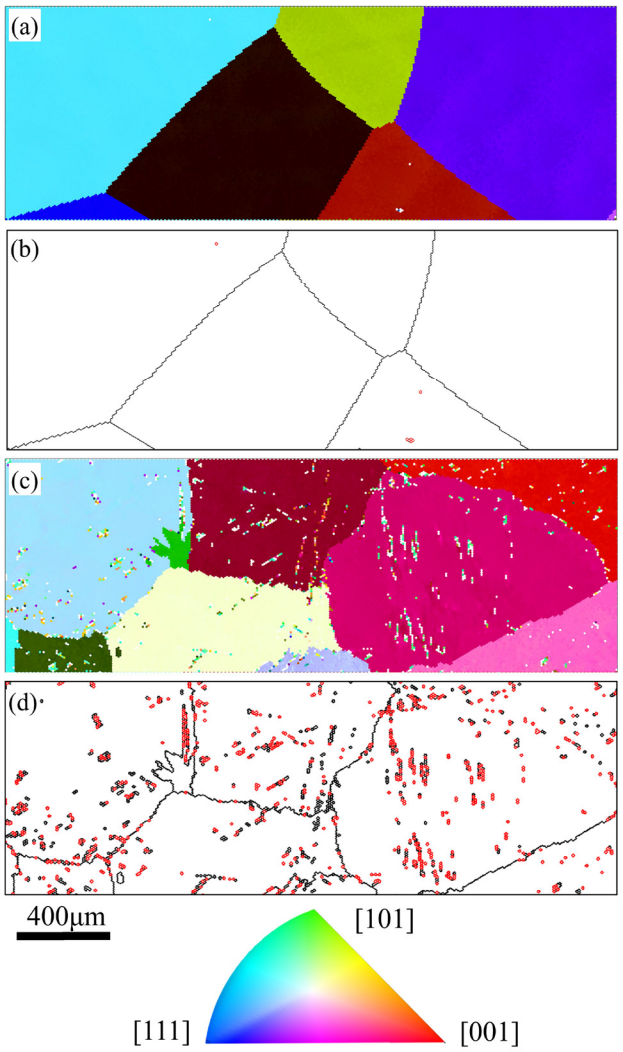

Fig. 4 Orientation maps of (a) 4N and (c) 3N samples, grain boundary maps and phase maps of (b) 4N and (d) 3N samples observed by means of EBSD. In (b) and (d). The areas surrounded by black lines represent base phases, and the areas surrounded by red lines represent the second phases.

4N (Fig. 4 (b)) but many of the second phases are precipitated in 3N indicated by the area surrounded by red lines in Fig. 4 (d). These phases are distributed in both grain and grain boundaries. Therefore, it can be stated here that the second phase is the main reason for the difference of hysteresis properties of the two samples, as well as the morphology difference of grain boundaries.

The specific morphology of the precipitates were investigated by STEM and its results are shown in Fig. 5. The overall view in Fig. 5 (a) indicates that the precipitates exist at a state of thin elongated columnar structures and aligned with each other in parallel. More specific observation in Fig. 5 (b) indicates that these precipitates grow in the grain as insertions, with a similar width of approximately 50 nm. The EDS results (center of Fig. 5) show that the carbon atoms are enriched in the precipitates, which can be considered as carbon compounds. These compounds can act as strong pinning obstacles against the structures and motion of domain wall, as demonstrated in the following section.

3.2. Domain structure

The hysteresis loss is the energy dissipated in the domain wall motion, therefore, it is important to clarify the condition of domain structures in both of the samples. Fig. 6 gives the demagnetized surface domain structures in part of each sample, from which it can be found that small complex lancet domain patterns dominates in the observed areas, and size of both surface domains are in the same order of magnitude.

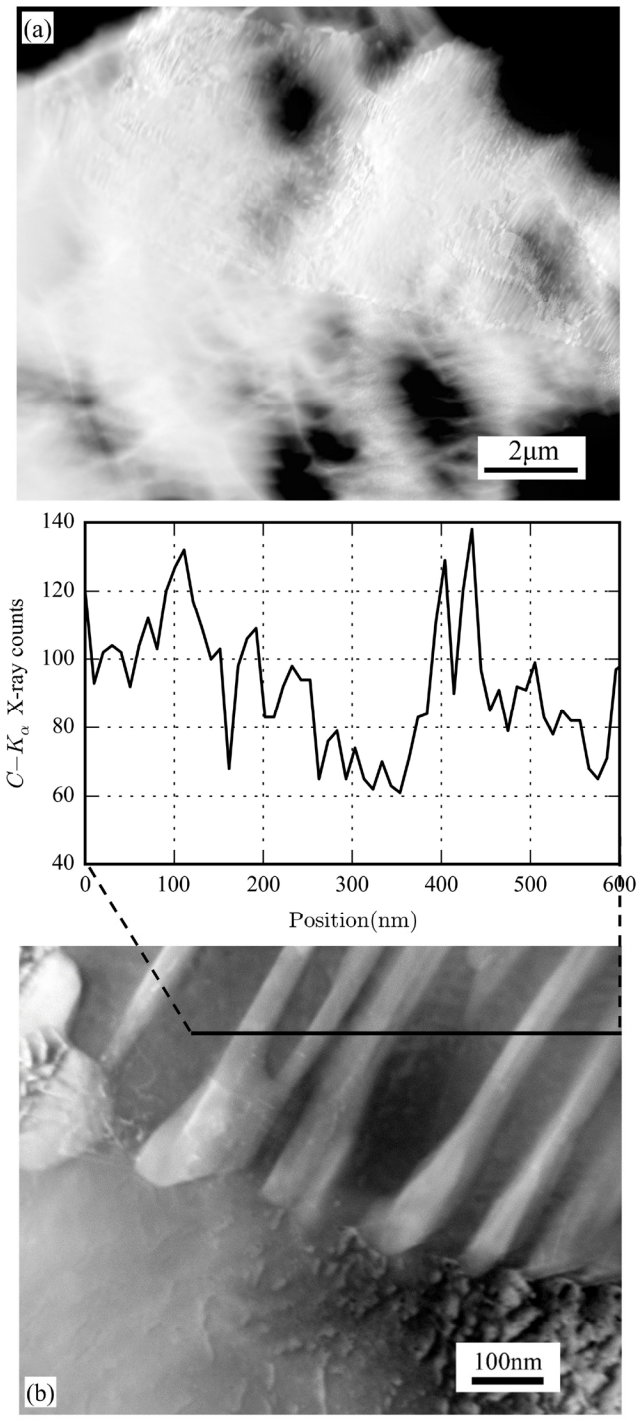

Fig. 5 The precipitates observed in the 3N by STEM high-angle annular dark-field (HAADF). (a) Observation in a wider area indicates high density of thin elongated phase, and (b) one more specific observed area in (a). The middle figure shows the EDS mapping of carbon element along the line in (b).

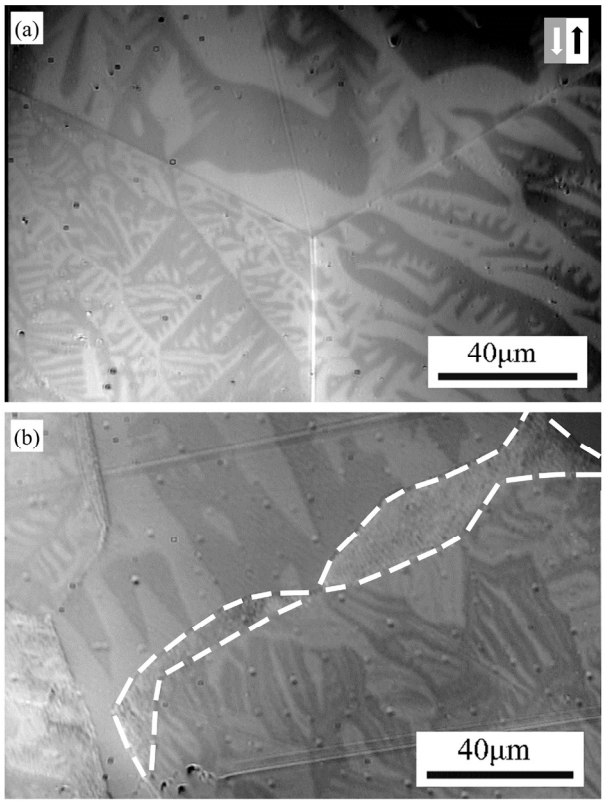

Fig. 6 The demagnetized domain structures of (a) 4N and (b) 3N samples observed by means of Kerr microscopy. The dark and bright areas indicate upward and downward magnetization components, respectively. The area surrounded by white dash lines in (b) indicate the carbon precipitates.

This proves that the precipitates dominate the difference in the hysteresis loss of the two samples, regardless of the influence of surfaces. The precipitates exist as non-magnet because no domain structures are observed in them (indicated by the arrows in Fig. 6). These non-magnetic precipitates weaken the interaction between magnetic components in the samples, resulting in the degradation of the magnetization process, which leads to the increase of hysteresis loss and reduction of permeability, which has been described previously.

It can be also found that domain structures in each individual grain of each sample differ. This kind of differences are mainly dominated by the deviation angle of the closest easy magnetization axis {001} from the sample surface, which has been reported in detail by Williams et al [5].

4. Conclusions

The hysteresis properties, specifically the relationship between hysteresis loss and maximum magnetic flux density, and magnetic domain of high purity Fe- 4 wt% Si (4N) alloy with comparison to Fe- 0.1 wt% - 4 wt% Si (3N) carbon created by CCLM were investigated.

1. High purity 4N alloy has super low coercivity, permeability and hysteresis loss than 3N, due to pinning of domain 180° and 90° wall displacement by the elongated thin carbon compounds which are distributed in both of grains and grain boundaries.
2. By increasing the purity of Fe-4 wt% Si, the relationship between hysteresis loss and maximum flux density are correlated linearly, by comparison to the nonlinear relationship in 3N.
3. The presence of carbon compounds precipitated in the grain boundaries changes the morphology of the grain boundaries. The compounds also retard the continuity of the domain structures, thus finally resulting in degradation of the hysteresis properties.

Acknowledgements This work were supported in part by the Nanotechnology Support Project of the Ministry of Education, Culture, Sports, Science, and Technology (MEXT). We also thank the support of Division of Instrumental Analysis Natural Science Center for Research and Education, Kagoshima University, Japan, especially numerous contributions of researcher Shingo Kubo at this center.

References

1) C. Kaido, T. Ogawa, Y. Arita, J. Yamasaki, and Y. Shishido: *J. Magn. Soc. Jpn.*, pp. 316-321, **31**, 4(2007) [in Japanese].
2) M. Gallaugher, N. Brodusch, R. Gauvin, and R. R. Chromik: *Ultramicroscopy*, pp. 40–49, 142(2014).
3) S. Szymura, C. Adamczyk, H. Majchrzak, J. Mehlis, and A. Zawada: *J. Mater. Sci. Lett.*, pp. 1259–1260, **6,** 11(1987).
4) K. C. Liao. *Metall. Trans. A*, pp. 1259– 1266, **17**, 8(1986).
5) H. Williams, R. Bozorth, and W. Shockley: *Phys. Rev.* pp. 155-178, **75**, 1(1949).
6) G. L. Houze: *J. Appl. Phys.,* pp. 1089-1096, **38**, 3(1967).
7) A. G. Tobin: *J. Appl. Phys.*, pp. 3611-3614, **40**, 9(1969).
8) J. Shilling and G. Houze: *IEEE Trans. Magn.*, pp. 195-223, **10**, 2(1974).
9) A. Morita, H. Fukui, H. Tadano, S. Hayashi, J. Hasegawa, and M. Niinomi: *Mater. Sci. Eng., A*, pp. 208-213, **280**, 1(2000).
10) K. Ono, T. Ogawa, and T. Sen: *Research paper of Industry Technology Center in Fukuoka,* pp. 99–103, 9(1999) [in Japanese].
11) T. Ogawa, Y. Ono, H. Koga, and K. Abiko: *Research paper of Industry Technology Center in Fukuoka*, 12(2001) [in Japanese].
12) F.J.G Landgraf, M Emura, J.C Teixeira, and M.F de Campos: *J. Magn. Magn. Mater.*, pp. 97-99, 215(2000)

Received Jul. 28, 2015; Revised Sep. 24, 2015; Accepted Oct. 22, 2015